https://doi.org/10.5194/essd-2024-245
Preprint. Discussion started: 1 October 2024


Open Access Earth System Science Data Discussions

# The SAIL dataset of marine atmospheric electric field observations over the Atlantic Ocean

Susana Barbosa[1], Nuno Dias[1,2], Carlos Almeida[1,2], Guilherme Amaral[1,2], António Ferreira[1,2], António Camilo[3], and Eduardo Silva[1,2]

[1]INESC TEC - INESC Technology & Science, Porto, Portugal
[2]ISEP, Instituto Superior de Engenharia do Porto, Porto
[3]CINAV. Marinha, Lisboa, Portugal

**Correspondence:** Susana Barbosa (susana.a.barbosa@inesctec.pt)

**Abstract.**

A unique dataset of marine atmospheric electric field observations over the Atlantic Ocean is described. The data are relevant not only for atmospheric electricity studies, but more generally for studies of the Earth's atmosphere and climate variability, as well as space-earth interactions studies. In addition to the atmospheric electric field data, the dataset includes simultaneous measurements of other atmospheric variables, including gamma radiation, visibility, and solar radiation. These ancillary observations not only support interpretation and understanding of the atmospheric electric field data, but are also of interest in themselves. The entire framework from data collection to final derived datasets has been dully documented to ensure traceability and reproducibility of the whole data curation chain. All the data, from raw measurements to final datasets, are preserved in data repositories with a corresponding assigned DOI. Final datasets are available from the Figshare repository (https://figshare.com/projects/SAIL_Data/178500) and computational notebooks containing the code used at every step of the data curation chain are available from the Zenodo repository (https://zenodo.org/communities/sail).

## 1 Introduction

The atmospheric electric field is an ever-present feature of the Earth's atmosphere, originated from the approximately 1,000 thunderstorms active at any given time on Earth (Rycroft et al., 2000).The strong air currents inside a thunderstorm cloud and the vertical movement of water and ice particles causes the separation of electric charges and an electric current to flow up to the ionosphere. Since the surface of the Earth and the ionosphere are good conductors, while the atmosphere is a reasonably good electrical insulator, an electric current flows through the majority of the Earth's atmosphere in the "fair weather" region remote from thunderstorms, and through the Earth's crust, constituting Earth's global electrical circuit (e.g Markson (2007); Rycroft et al. (2008); Williams (2009)). The small density current flowing between the ionosphere and the Earth's surface is only of the order of a picoampere per square meter ($10^{-12}$ Am$^{-2}$) but it is able to produce a vertical electric field between 100 and 300 Vm$^{-1}$ near ground level (e.g. Burns et al. (2012)).

The global atmospheric electric field exhibits diurnal variability driven by the daily variation of thunderstorm activity throughout the Earth, influenced by the tropical distribution of land masses, above which thunderstorms preferentially form at

https://doi.org/10.5194/essd-2024-245
Preprint. Discussion started: 1 October 2024




the end of the day (Wilson, 1921). The global nature of the Earth's electric field, and its diurnal variability, were confirmed by data collected in a series of campaigns aboard the *Carnegie* vessel between 1915 and 1929, showing that the electric field exhibits a diurnal variation, reaching its highest values at 19:00 UTC, regardless of the location on the globe (Parkinson, 1931; Torreson, 1946). This diurnal variation became to be known as the "Carnegie curve", and it is used to this day as the reference for the diurnal variation of the global atmospheric electric field (Harrison, 2013, 2020).

This diurnal feature of the global atmospheric electric field is hard to observe in non-marine measurements of the electric field, as it is usually hidden by local sources of variability. Marine measurements of the atmospheric electric field are therefore very relevant, but rare. And in a climate change context the need of such observations is even more compelling, as the electrical conductivity of the ocean air is clearly linked to global atmospheric pollution and aerosol content (Price, 1993; Rycroft et al., 2000; Harrison, 2004). Measurements from the research vessel *Oceanographer* in 1967 indicated values of atmospheric electrical conductivity consistent with the original Carnegie observations in the remote South Pacific, but a decrease over the Atlantic of at least 20%,which was attributed to an increase in North hemisphere aerosol pollution (Cobb and Wells, 1970). Here we present a unique dataset of atmospheric electric field measurements performed over the Atlantic Ocean in the scope of the SAIL (Space-Atmosphere-ocean Interactions in the marine boundary Layer) project (Barbosa et al., 2023d). Section 2 gives an overview of the monitoring campaign and methodology for collecting the data, section 3 describes the dataset and applied quality assurance procedures, and concluding remarks are provided in section 4.

## 2 Monitoring campaign

The SAIL monitoring campaign started on January 5th 2020 aboard the Portuguese navy ship *NRP Sagres* for an initially planned circum-navigation expedition of 371 days. However, the voyage was interrupted due to the covid pandemic, and the campaign was thus restricted to the Atlantic Ocean. Figure 1 depicts the ship's trajectory during the SAIL campaign. After a short stop at Cape Town for provisions, the ship departed the same day back to Portugal, having arrived to Lisboa on May 10th, after a required technical stop for repairs at Cabo Verde.

The monitoring system of the SAIL campaign is described in detail in Barbosa et al. (2022c). In brief, the atmospheric electric field and ancillary variables are measured on the mizzen mast of the *NRP Sagres* ship and transmitted to a dedicated on-board computer. Every measurement is tagged with a timestamp with microsecond precision based on the system clock in coordinated universal time (UTC). The system clock is corrected by a PPS (Pulse Per Second) signal available from a Global Navigation Satellite System (GNSS) receiver.

The atmospheric electric field is measured near the top of the ship's mast, at about 20 meters height, with an automatic electric field meter sensor CS-110 (Campbell Scientific, UK) measuring the vertical component of the electric field by means of a rotating grounded shutter. A secondary measurement is performed at the same mast but closer to the ship deck, at an height of around 5 meters, using an identical instrument. Ancillary atmospheric variables are measured close to the main electric field sensor, at the 20 meters height, and include gamma radiation, visibility, and short-wave solar radiation. Gamma radiation resulting from natural radioactivity, including the radioactive decay of radon gas progeny, and from the interaction of cosmic

https://doi.org/10.5194/essd-2024-245
Preprint. Discussion started: 1 October 2024


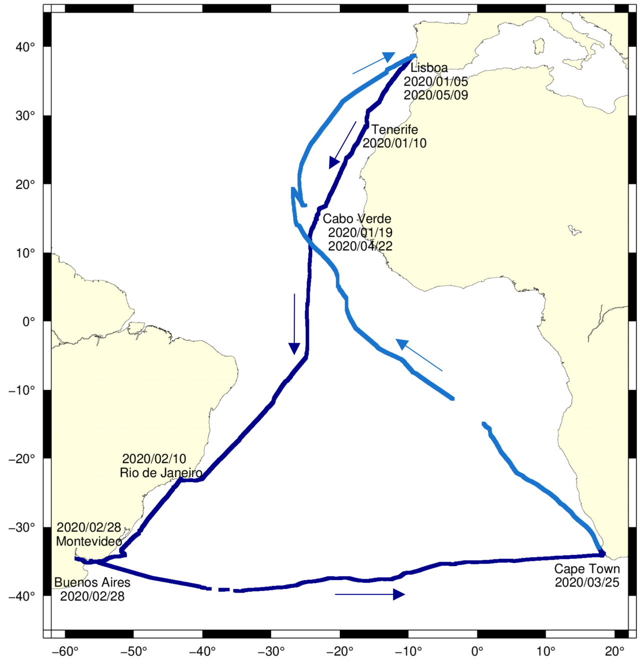


**Figure 1.** Trajectory of the *NRP Sagres* ship from January to May 2020; blanks correspond to periods with no data.

rays and atmospheric gas molecules, is a direct source of atmospheric ions. Ions influence cloud and aerosol processes (Harrison and Carslaw, 2003) and changes in ion concentration and/or ion mobility impact the local atmospheric electric field by changing atmospheric conductivity (Harrison and Tammet, 2008). Visibility and solar radiation are used to assess atmospheric conditions, as weather conditions causing changes in charge distribution or ion mobility influence the local atmospheric field (e.g. Bennett and Harrison (2007)).

Gamma radiation is measured with a 76 × 76 mm$^2$ NaI(Tl) cylindrical scintillator (Scionix, the Netherlands) equipped with an electronic total count single channel analyzer measuring total counts of gamma radiation in the 475 keV to 3 MeV energy range (Zafrir et al., 2011). The scintillator is encased in a water-proof container protecting it from the harsh marine conditions and installed next to the electric field instrument (starboard side), in an upright position and pointing upwards. Visibility is measured at the port side with a visibility sensor SWS050 (Biral, UK) providing meteorological optical range measurements in the range from 10 m to 40 km. Short-wave solar radiation is measured next to the electric field sensor using incoming (Apogee, SP-510) and outgoing (Apogee, SP-610) solar radiation sensors. Local meteorological information (rain, atmospheric pressure, temperature, and wind) is manually recorded by the ship's crew every 1 hour as part of the navy's operations routine (meteorological information is not recorded when the ship is not navigating).

During the 126-days of the SAIL campaign, all measurements were performed continuously at a rate of 1Hz, except for visibility with measurements every 1-minute. Overall data completion is $> 95\%$. Data loss due to malfunction of the monitoring system occurred on 8th and 9th March (during the trip from Buenos Aires to Cape Town) and then from 4 to 6 April (in the

https://doi.org/10.5194/essd-2024-245
Preprint. Discussion started: 1 October 2024


leg from Cape Town to Lisboa), due to issues on the onboard computer and storage systems. The voids in the ship's trajectory represented in Figure 1 correspond to these data gaps. The data management strategy for all the data collected in the scope of the SAIL campaign is detailed in the SAIL data management plan (Barbosa and Karimova, 2021).

## 3 Data and quality assurance

All the data from the SAIL campaign are preserved in order to foster its reuse in different scientific domains and to enable initially unforeseen uses of the data. All data handling processes are fully documented to ensure traceability and reproducibility.

The raw campaign data (Barbosa et al., 2021) are only available upon request due to its large size (around 700 GB). This dataset of raw measurements includes the data obtained directly from the ship on-board system (designated as ship data), the data (designated as sensor data) obtained from the ship data by correcting logging errors (Amaral and Dias, 2021) and the data (designated as geosensor data) obtained from the sensor data by adding two additional columns corresponding to latitude and longitude based on the GNSS data from the campaign (Ferreira, 2021)).

Data were collected continuously during the SAIL campaign, thus including both measurements performed over the ocean when the ship was sailing, as well as coastal measurements performed when the ship was docked during the different stops along its journey (see Figure 1). To facilitate the usage of the data for studies requiring ocean-only observations (e.g. Barbosa et al. (2023c)), a flag denoting fully-ocean days is added to the final datasets (Figure 2).

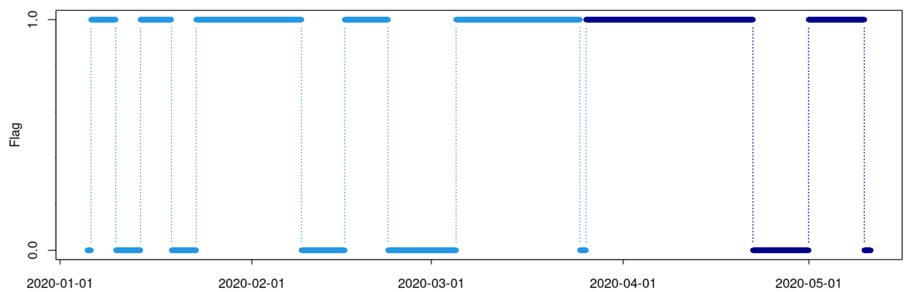


**Figure 2.** Flag distinguishing fully ocean (=1) and fully or partially land (=0) days. The same colours as in Figure 1 are used for the first leg of the ship trajectory and for the returning leg.

Pre-processed data (Barbosa et al., 2023a) are produced from the raw data by implementing quality-control and pre-processing procedures. These procedures and the resulting quality-assured derived datasets are described in section 3.1 for the atmospheric electric field data, and in section 3.2 for the ancillary data.

### 3.1 Atmospheric electric field

Measurements of the atmospheric electric field are performed with no site-specific corrections. The default value of the sensor (2 meter height) is used, both for the primary instrument and the secondary (lower) one, designated as E1 and E2, respectively. The behaviour of the two instruments is addressed in section 3.1.1.

https://doi.org/10.5194/essd-2024-245
Preprint. Discussion started: 1 October 2024


The raw atmospheric electric field data are first pre-processed for basic quality-control (section 3.1.2). Corrections are applied at a subsequent stage, and are fully documented, in order to be able to trace back all the steps to reproduce and/or to further modify the data processing (section 3.1.3). Selection of fair weather atmospheric electric field data is described in section 3.1.4.

### 3.1.1 Zero-field measurements

The two electric field instruments were factory-calibrated before the SAIL campaign, and further evaluated after the campaign in terms of zero-field measurements, by using a zero field cover plate attached to the instrument's shutter. The data were collected on land, at the same height, over three consecutive days (June 3 to 5, 2022). Figure 3 summarises the zero-field electric field measurements and Figure 4 the corresponding leakage current measurements. These results indicate that the primary electric field sensor has a smaller error and lower leakage current than the secondary sensor, but both sensors perform well, the difference to zero being below 4 V/m and leakage currents below 0.025 nA.

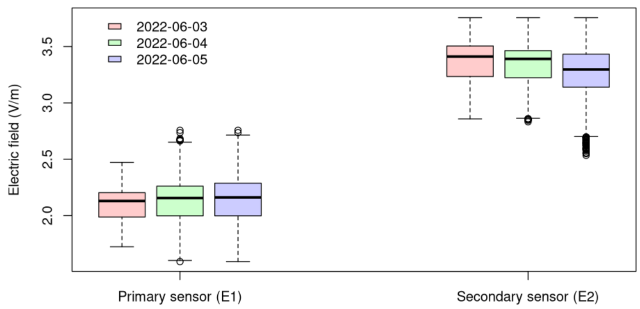


**Figure 3.** Zero-field electric field measurements.

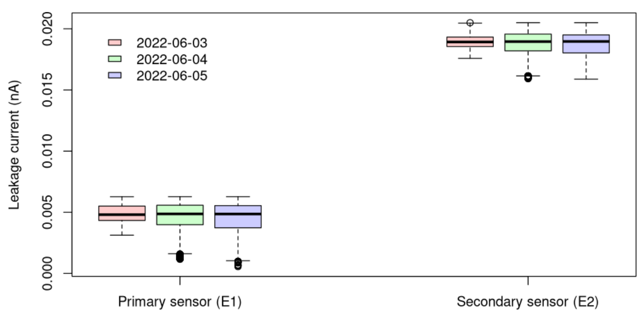


**Figure 4.** Zero-field leakage current measurements.

### 3.1.2 Atmospheric electric field data pre-processing

Pre-processing of the raw atmospheric electric field data is documented in Barbosa (2023c), and includes:

https://doi.org/10.5194/essd-2024-245
Preprint. Discussion started: 1 October 2024


- checking the instrument status code; if different than 1 (indicating good instrument health) the corresponding measurement is set as missing (flagged as NA);
- changing the sign of the atmospheric electric field measurements to comply with the sign convention denoting the potential gradient as positive under undisturbed atmospheric electrical conditions (e.g. Harrison and Nicoll (2018));
- averaging 1-second electric field measurements into 1-minute values;
- averaging geographical coordinates (taking into account angularity) to 1-minute averaged values;
- computing the standard deviation every 1–minute from the 1-second measurements;
- checking the record continuity and inserting a flag (NA) for missing times in order to ensure a continuous time series of atmospheric electric field observations.

The pre-processed dataset obtained by applying to the raw data these procedures (but before application of the corrections that will be described in section 3.1.3) is available from the INESC TEC data repository (Barbosa et al., 2023a).

Figure 5 presents examples of 1-minute pre-processed electric field observations from the two sensors for days with contrasting weather conditions. These examples emphasise the consistency of the temporal variability of the electric field measurements from the two sensors, on one hand, and on the other hand the large difference in the corresponding values of the atmospheric electric field, with values from the secondary instrument substantially lower and less variable than the ones of the primary instrument. These differences are not explainable by differences in the performance of the two instruments (see section 3.1.1) nor by differences in the height of the sensors, as these would not explain the reduced variability of the secondary electric field measurements. Plausibly the differences between primary and secondary electric field observations result from the location of the secondary sensor and consequent field distortion effects. While the primary sensor, near the top of the mast, has relatively unimpeded surroundings, the secondary (lower) sensor is adjacent to several structures of the ship, likely distorting the local electric field. Despite this difficulty the secondary electric field measurements, at the lower height, are kept in the dataset, but their use and interpretation should be cautious, particularly in terms of absolute values.

#### 3.1.3 Atmospheric electric field data corrections

**Height correction for primary electric field measurements**

The influence of the height at which the primary atmospheric electric field measurements are performed is assessed by considering simultaneous observations of the atmospheric electric field conducted at the height of about 20 meters near the top of the mast (using instrument E1) and at sea level (standard 2 meters height from the ground), with the secondary instrument (E2) placed on shore when the ship was docked at the Lisbon Naval Base. Due to logistic and operational constrains, the measurements were performed for a short period of about 2 hours on June 16th 2020, under fair weather conditions. These simultaneous measurements are presented in Figure 6. The temporal variability of the two measurements is consistent, but

https://doi.org/10.5194/essd-2024-245
Preprint. Discussion started: 1 October 2024


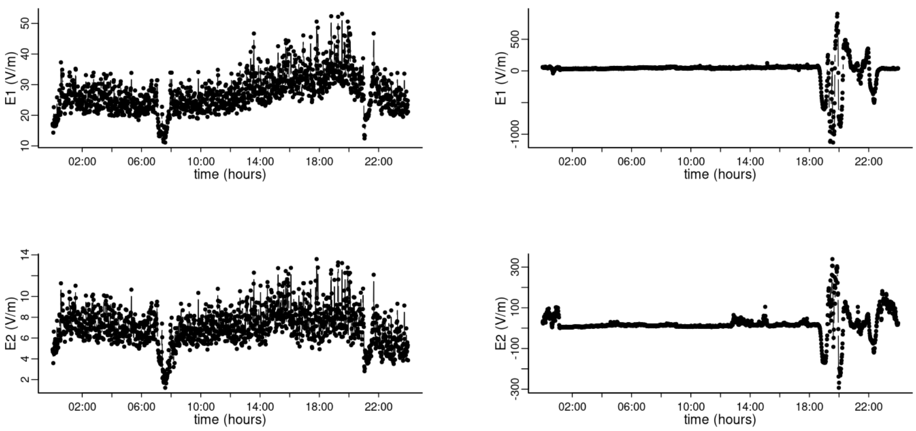


**Figure 5.** Examples of pre-processed electric field observations for a clear day (on February 2nd, left) and for a rainy day (on January 28th, right), from the primary (higher) instrument (top) and the secondary (lower) instrument (bottom).

there is a clear bias between the mast and the pier measurements, the mast measurements being significantly lower (averaging 68 V/m ) than the pier measurements (which average 119 V/m). The bias is estimated by means of a linear model, represented in Figure 7. The (positive) correlation between the two measurements is statistically significant and the fitted linear model has a slope equal to 1.76 ($\pm 0.013$), explaining $72\%$ of the variance. The linear model's intercept is zero (statistically not significant). These estimates are used for height correction of the primary measurements of the atmospheric electric field on the mast, by multiplying all the mast observations by 1.76: $E1_{h\_corr} = E1 \times 1.76$ (V/m).

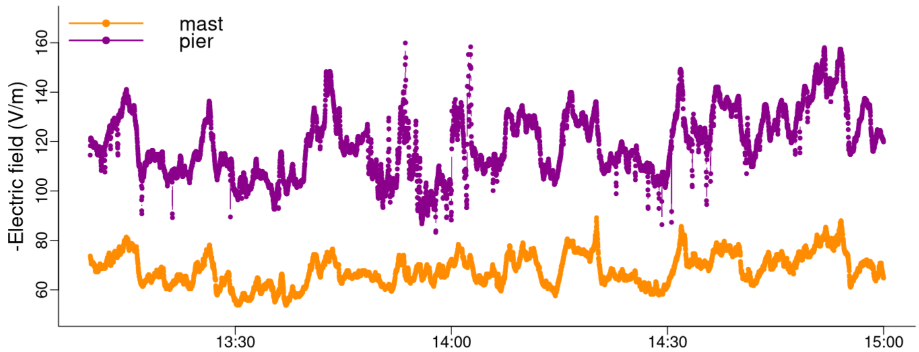


**Figure 6.** Time series of simultaneous atmospheric electric field measurements every 1-second performed at the mast of the ship (at a height of about 20 meters) and at the pier (at the standard height of 2 meters).

## Bias correction for secondary electric field measurements

Figure 8 summarises the height-corrected primary electric field observations and the secondary electric field measurements in terms of its daily median values (Figure 8, right) and in terms of daily median differences $E1_{h\_corr} - E2$ (Figure 8, left). The

https://doi.org/10.5194/essd-2024-245
Preprint. Discussion started: 1 October 2024


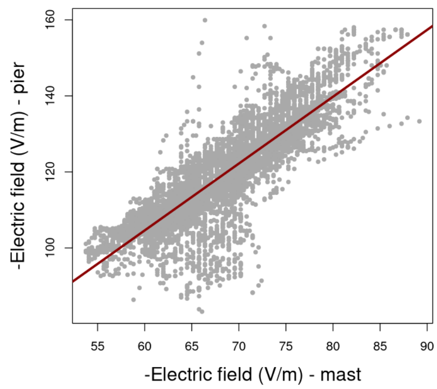


**Figure 7.** Scatterplot and fitted linear model for the observation represented in Figure 6.

differences are in general positive (primary measurements larger than secondary electric field measurements), averaging 56 V/m. This bias estimate is used to correct secondary electric field observations: $E2_{corr} = E2 + 56$ (V/m).

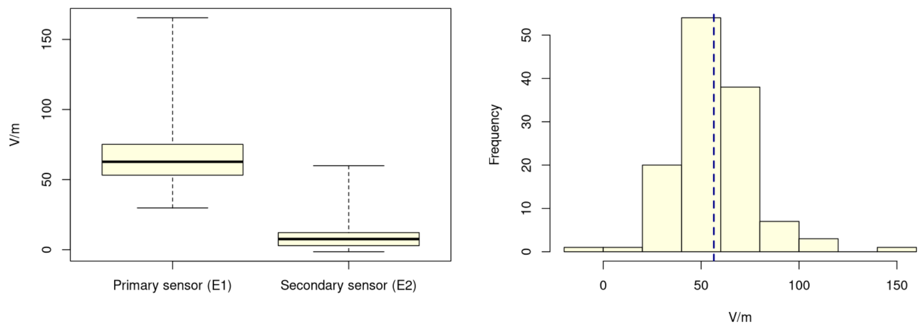


**Figure 8.** Daily median values of height-corrected primary electric field observations and secondary electric field measurements (left) and corresponding daily median differences $E1_{h\_corr} - E2$ (right), the dashed vertical line representing the average of the differences.

150 The datasets of height-corrected primary electric field observations and bias-corrected secondary electric field observations are available from the Figshare repository (Barbosa et al., 2024a).

### 3.1.4 Atmospheric electric field data selection

A dataset of selected atmospheric electric field observations is derived from the dataset of primary corrected electric field observations by applying the following data-driven criteria:

155 – Non-negative Potential Gradient values (corresponding to 98.6% of the observations);

– Observations flagged as fully-ocean day (see Figure 2) which correspond to 71.9 % of the observations.

https://doi.org/10.5194/essd-2024-245
Preprint. Discussion started: 1 October 2024


In addition to these criteria, the following fair weather criteria (Harrison and Nicoll, 2018) are applied based on the available ancillary and meteorological information (see section 3.2):

- Dry day, according to manual precipitation records (corresponding to 85.8% of the days);
- Clear sky (meteorological optical range $\geq 30,000$ meters), a condition fulfilled by 60.1 % of the observations.

The application of these criteria results in retaining 35.6 % of the corrected primary electric field observations. The resulting dataset of fair weather marine observations of the atmospheric electric field is available from the Figshare repository (Barbosa et al., 2024b).

Figure 9 shows the hourly boxplots for the selected fair weather electric field observations. The Sagres data display the typical *Carnegie curve* shape, with minimum around 04:00 UTC and maximum around 19:00 UTC, but the amplitude of the curve represented by hourly median values is smaller.

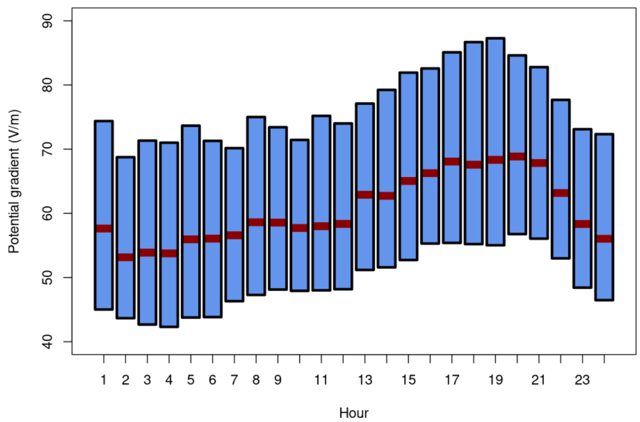


**Figure 9.** Hourly boxplots of SAIL fair weather atmospheric electric field observations. The horizontal red line represents the hourly median value of the potential gradient.

### 3.2 Ancillary observations

#### 3.2.1 Gamma radiation

Pre-processed gamma radiation data are obtained from the raw data by aggregating 1-second counts to 1-minute values, calculating average geographical coordinates every 1-minute, and by checking data continuity and flagging missing measurements, which correspond to $4.4\%$ of the time series values. Further quality-control is performed by inspecting the pre-processed 1-minute data, and identifying anomalous values, typically sharp spikes (lasting less than 3 minutes), and anomalously low values before/after a data gap (associated with recovery of the instrument after power failure). These outliers ($1.2\%$ of the time series values) are set as missing, as exemplified in Figure 10. The jupyter notebook implementing these pre-processing and quality-

https://doi.org/10.5194/essd-2024-245
Preprint. Discussion started: 1 October 2024


control steps is preserved in Zenodo (Barbosa (2024a)). The resulting dataset of quality-assured gamma radiation observations is available from Figshare (Barbosa et al., 2022a).

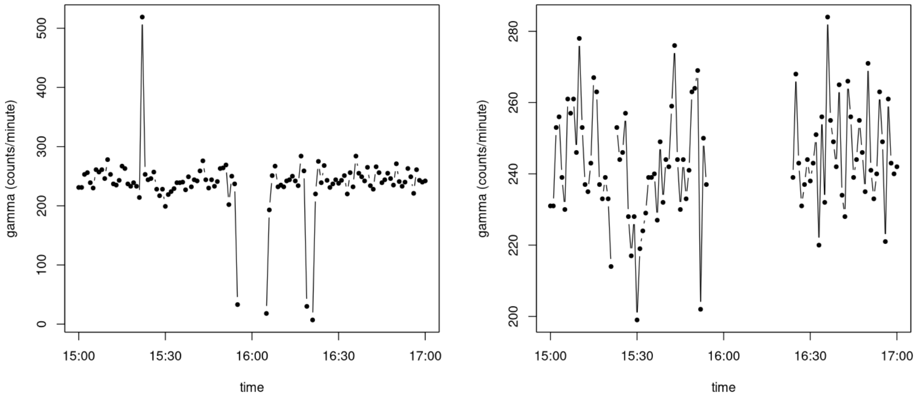


**Figure 10.** Example (16th January 2020) of pre-processing of 1-minute gamma radiation observations: spikes and anomalously low values before/after a data gap (left) are set as missing (right).

### 3.2.2 Visibility

Pre-processed data are obtained by extracting meteorological optical range measurements from the raw visibility data and then checking temporal continuity and inserting a flag (NA) for missing observations, in order to produce a continuous time series (Barbosa, 2024b). The quality-assured time series of meteorological optical range observations is available from the Figshare repository (Barbosa et al., 2022b).

The meteorological optical range measured by the visibility sensor reflects the transparency of the atmosphere, and is an useful parameter to assess local atmospheric conditions. As an example, Figure 11 displays the visibility data for a clear day and for a rainy day. In the first case visibility values are consistently high, except for cloudy conditions reducing visibility around 08:00, while in the latter case visibility values are low, with lowest observations around 17:00 and 19:00, associated with rain episodes.

### 3.2.3 Solar radiation

Raw solar radiation data every 1-second are pre-processed to produce 1-minute averaged incoming and outgoing short-wave solar radiation. Inspection of the data for quality-control reveals the existence of non-valid negative values of solar radiation. These negative (and small magnitude) values of solar radiation are replaced by zero. Inspection of the incoming solar radiation data for each hour of the day reveals a few small values during night hours, which are set as zero. A much larger number of non-zero night values is found in the case of outgoing radiation - likely reflecting the effect of the ship's own illumination - and these values are set as missing. The jupyter notebooks implementing these quality-control procedures are preserved in

https://doi.org/10.5194/essd-2024-245
Preprint. Discussion started: 1 October 2024

Open Access Earth System Science Data Discussions

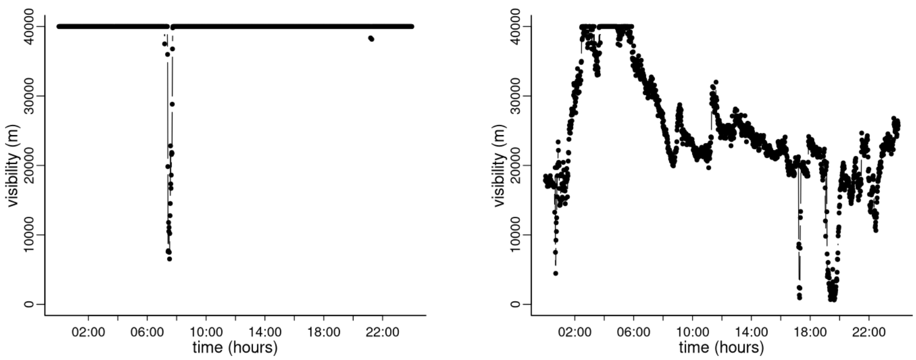


**Figure 11.** Example of visibility observations for a clear day (on February 2nd, left) and for a rainy day (on January 28th, right).

the Zenodo repository (Barbosa, 2023d). The resulting quality-assured datasets of incoming and outgoing short-wave solar radiation are available from the Figshare repository (Barbosa et al., 2023b).

Figure 12 displays an example of the daily variability of 1-minute incoming solar radiation observations for the same days as in Figure 11. For the sunny day the diurnal pattern is more regular and incoming solar radiation values are higher. It must be noted that although the solar radiation sensors were installed high on the mast, some partial shading and/or enhanced reflection by the ship's sails cannot be discarded.

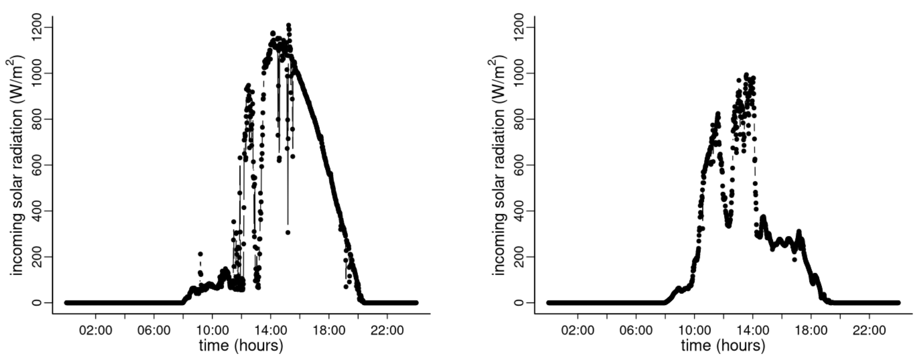


**Figure 12.** Example of incoming short-wave solar radiation observations for a clear day (on February 2nd, left) and for a rainy day (on January 28th, right).

### 3.2.4 Meteorological information

Local meteorological information is collected every hour by meteorological observers of the ship's crew (Table 1). The raw data (Camilo, 2021) were corrected by homogenising non-standard missing values flags and by removing headers and formatting features in order to enable further automatic processing. The resulting corrected data (Barbosa, 2023b) are subject to further quality-control procedures specific to each meteorological parameter, as detailed in the jupyter notebook made available in

https://doi.org/10.5194/essd-2024-245
Preprint. Discussion started: 1 October 2024


**Table 1.** Meteorological data over the Atlantic Ocean collected onboard the NRP Sagres ship during the SAIL campaign.

| Datafile column | Meteorological variable | Unit / format |
|---|---|---|
| 1 | Date | yyyy-mm-dd |
| 2 | Time | HH:MM, local time |
| 3 | Latitude | DD° M.M |
| 4 | Latitude | suffix (N or S) |
| 5 | Longitude | DDD° M.M |
| 6 | Longitude | suffix (E or W) |
| 7 | QNH (Query Nautical Height) | mbar |
| 8 | Temperature - dry | °C |
| 9 | Temperature - wet | °C |
| 10 | Dew point | °C |
| 11 | Relative humidity | % |
| 12 | Water temperature - bucket | °C |
| 13 | Water temperature - hull | °C |
| 14 | True wind direction | ° |
| 15 | True wind speed | knots |
| 16 | True wind force | beaufort scale |
| 17 | Wave direction | compass half-wind |
| 18 | Wave height | m |
| 19 | Visibility | qualitative code [1] |
| 20 | Cloud cover | oktas |
| 21 | Precipitation | qualitative code [1] |

[1] excellent, very good, good, moderate, poor

[2] moderate, light, drizzle, drizzle moderate, drizzle light

Zenodo (Barbosa, 2023a). These include, in addition to removal of obvious outliers, the translation of visibility classes from Portuguese to English based on WMO-No. 471 (WMO, 2018), and the homogenisation and translation of qualitative precipitation information. The resulting quality-assured dataset of meteorological observations is available from the Figshare repository (Barbosa and Camilo, 2023).

## 4 Conclusions

The SAIL dataset of marine atmospheric electric field observations over the Atlantic Ocean is a unique dataset, relevant not only for atmospheric electricity studies, but more generally for studies of the Earth's atmosphere and climate variability, as well as space-earth interactions studies.

https://doi.org/10.5194/essd-2024-245
Preprint. Discussion started: 1 October 2024


Open Access Earth System Science Data Discussions

**Table 2.** Code (Jupyter notebook) available on the project SAIL community on Zenodo (https://zenodo.org/communities/sail/).

| Title | DOI | Reference |
|---|---|---|
| Pre-processing and quality-control of of electric field data | 10.5281/zenodo.10276613 | Barbosa, 2023c |
| Pre-processing and quality-control of gamma radiation data | 10.5281/zenodo.11620014 | Barbosa, 2024a |
| Pre-processing of visibility data | 10.5281/zenodo.11621789 | Barbosa, 2024b |
| Pre-processing and quality-control of solar radiation data | 10.5281/zenodo.10161091 | Barbosa, 2023d |
| Pre-processing of meteorological data | 10.5281/zenodo.10150266 | Barbosa, 2023a |

In addition to the atmospheric electric field measurements, the data presented here includes simultaneous measurements of other atmospheric variables, including gamma radiation, visibility, and solar radiation. These ancillary data not only support interpretation and understanding of the atmospheric electric field observations, but are of interest in themselves (e.g. Barbosa et al. (2023c)), as data seldom measured over the ocean, and even more rarely at the spatial and temporal resolutions achieved in the SAIL campaign.

The measurement of the atmospheric electric field on a tall ship has several challenging aspects, including the variable site geometry, particularly related to the changing configuration of the sails, and field distorting effects due to the ship's structures. Corrections have been provided according to the best available information, but the mentioned limitations can still influence absolute values of the atmospheric electric field. Enhanced confidence is ensured by relative atmospheric electric field values.

The entire framework from data collection to final derived datasets has been dully documented in order to foster reproducibility of the whole data curation chain, and enable alternative data processing strategies and different corrections to be seamlessly implemented.

A follow-up monitoring of the atmospheric electric field aboard the NRP Sagres ship is currently ongoing, and corresponding datasets will be updated in a future effort.

## 5 Code and data availability

All the code and data is publicly available. The project SAIL community on Zenodo (https://zenodo.org/communities/sail/) contains the technical documents related to the SAIL data, and the computational (jupyter) notebooks used at the different stages of data processing (Table 2). Raw data (Barbosa et al. (2021), DOI: 10.25747/b2ff-kg31) and pre-processed data (Barbosa et al. (2023a), DOI: 10.25747/58P6-6B76) are available from INESC TEC RDM repository. Final datasets (Table 3) are available from the Figshare repository, under the SAIL data project (https://figshare.com/projects/SAIL_Data/178500).

*Author contributions.* SB: conceptualization, data curation, formal analysis, writing - original draft; ND, GA, AF: set-up of monitoring system, data collection; data curation; CA: set-up of monitoring system, data collection; AC, ES: resources, supervision.

https://doi.org/10.5194/essd-2024-245
Preprint. Discussion started: 1 October 2024




**Table 3.** Datasets available on the SAIL data project on Figshare (https://figshare.com/projects/SAIL_Data/178500).

| Title | DOI | Reference |
|---|---|---|
| Atmospheric electric field data | 10.6084/m9.figshare.19692391.v1 | Barbosa et al., 2024a |
| Fair weather atmospheric electric field data | 10.6084/m9.figshare.26022001.v1 | Barbosa et al., 2024b |
| Gamma radiation data | 10.6084/m9.figshare.20393931.v3 | Barbosa et al., 2022a |
| Visibility data | 10.6084/m9.figshare.19692394.v3 | Barbosa et al., 2022b |
| Solar radiation data | 10.6084/m9.figshare.24614754.v1 | Barbosa et al., 2023b |
| Meteorological data | 10.6084/m9.figshare.24613869.v1 | Barbosa and Camilo, 2023 |

*Competing interests.* The authors declare absence of competing interests.

*Acknowledgements.* The support provided by the NRP Sagres's crew and the Portuguese Navy is gratefully acknowledged. Project SAIL received funding from the Portuguese Ministry of Environment and Energy Transition through Fundo Ambiental protocol no 9/2020 and by the Portuguese Foundation for Science and Technology (FCT) LA/P/0063/2020.

https://doi.org/10.5194/essd-2024-245
Preprint. Discussion started: 1 October 2024




## References

Amaral, G. and Dias, N.: SAIL campaign - Technical report on Sensor Data correction, https://doi.org/10.5281/zenodo.4518865, 2021.

Barbosa, S.: SAIL Jupyter Notebooks - Pre-processing of meteorological data from the SAIL project, https://doi.org/10.5281/zenodo.10150266, 2023a.

Barbosa, S.: Sagres ship corrected meteorological data 2020 [dataset], https://doi.org/10.25747/FYKZ-9H72, 2023b.

Barbosa, S.: SAIL Jupyter Notebooks - Pre-processing and quality-control of electric field data from the SAIL project, https://doi.org/10.5281/zenodo.10276613, 2023c.

Barbosa, S.: SAIL Jupyter Notebooks - Pre-processing and quality-control of solar radiation data from the SAIL project, https://doi.org/10.5281/zenodo.10161091, 2023d.

Barbosa, S.: SAIL Jupyter Notebooks - Pre-processing and quality-control of gamma radiation data from the SAIL project, https://doi.org/10.5281/zenodo.10134222, 2024a.

Barbosa, S.: SAIL Jupyter Notebooks - Pre-processing of visibility data from the SAIL project, https://doi.org/10.5281/zenodo.11621789, 2024b.

Barbosa, S. and Camilo, A.: SAIL - Meteorological data, https://doi.org/10.6084/m9.figshare.24613869.v1, 2023.

Barbosa, S. and Karimova, Y.: SAIL Data Management Plan, https://doi.org/10.5281/zenodo.4286209, 2021.

Barbosa, S., Almeida, C., Amaral, G., Dias, N., Ferreira, A., Almeida, J. M., Camilo, A., David, G., Karimova, Y., Lima, L., Martins, A., Oliveira, R., Ribeiro, C., Silva, I., and Silva, E.: Raw data collected onboard the Sagres ship during the SAIL project campaign [dataset], https://doi.org/10.25747/b2ff-kg31, 2021.

Barbosa, S., Almeida, C., Amaral, G., Dias, N., Ferreira, A., Camilo, A., and Silva, E.: SAIL - gamma radiation data [dataset], https://doi.org/10.6084/m9.figshare.20393931.v3, 2022a.

Barbosa, S., Almeida, C., Amaral, G., Dias, N., Ferreira, A., Camilo, A., and Silva, E.: SAIL - Visibility data [dataset], https://doi.org/10.6084/m9.figshare.19692394.v3, 2022b.

Barbosa, S., Dias, N., Almeida, C., Amaral, G., Ferreira, A., Lima, L., Silva, I., Martins, A., Almeida, J., Camilo, M., and Silva, E.: An holistic monitoring system for measurement of the atmospheric electric field over the ocean - the SAIL campaign, in: OCEANS 2022 - Chennai, p. 1–5, https://doi.org/10.1109/OCEANSChennai45887.2022.9775273, 2022c.

Barbosa, S., Almeida, C., Amaral, G., Dias, N., and Ferreira, A.: Pre-processed atmospheric data from the SAIL campaign onboard the Sagres ship [Data set], https://doi.org/10.25747/58P6-6B76, 2023a.

Barbosa, S., Almeida, C., Amaral, G., Dias, N., Ferreira, A., Camilo, A., Silva, E., and Coelho, L.: SAIL - Solar radiation data, https://doi.org/10.6084/m9.figshare.24614754.v1, 2023b.

Barbosa, S., Dias, N., Almeida, C., Silva, G., Ferreira, A., Camilo, A., and Silva, E.: Precipitation-Driven Gamma Radiation Enhancement Over the Atlantic Ocean, J Geophys Rese-Atmos, 128, e2022JD037 570, https://doi.org/10.1029/2022JD037570, 2023c.

Barbosa, S., Dias, N., Amaral, G., Ferreira, A., Almeida, C., and Maurício Camilo, A.: SAILing to research Earth's climate , INESC TEC Science & Society, 1, https://science-society.inesctec.pt/index.php/inesctecesociedade/article/view/114, 2023d.

Barbosa, S., Almeida, C., Amaral, G., Dias, N., Ferreira, A., Camilo, A., and Silva, E.: SAIL - Atmospheric electric field data, https://doi.org/10.6084/m9.figshare.19692391.v1, 2024a.

Barbosa, S., Almeida, C., Amaral, G., Dias, N., Ferreira, A., Camilo, A., and Silva, E.: SAIL - Fair weather atmospheric electric field data, https://doi.org/10.6084/m9.figshare.26022001.v1, 2024b.

https://doi.org/10.5194/essd-2024-245
Preprint. Discussion started: 1 October 2024



Bennett, A. J. and Harrison, R. G.: Atmospheric electricity in different weather conditions, Weather, 62, 277–283, https://doi.org/10.1002/wea.97, 2007.

Burns, G., Tinsley, B., Frank-Kamenetsky, A., Troshichev, O., French, W., and Klekociuk, A.: Monthly diurnal global atmospheric circuit estimates derived from Vostok electric field measurements adjusted for local meteorological and solar wind influences, J Atmos Sci, 69, 2061–2082, 2012.

Camilo, A.: Sagres ship meteorological data 2020 [dataset], https://doi.org/10.25747/rp31-kf14, 2021.

Cobb, W. E. and Wells, H. J.: The electrical conductivity of oceanic air and its correlation to global atmospheric pollution, J Atmos Sci, 27, 814–819, 1970.

Ferreira, A.: SAIL campaign - Technical report on GNSS Post- processing, https://doi.org/10.5281/zenodo.4447619, 2021.

Harrison, R. and Nicoll, K.: Fair weather criteria for atmospheric electricity measurements, J Atmos Solar-Terr Phy, 179, 239–250, https://doi.org/10.1016/j.jastp.2018.07.008, 2018.

Harrison, R. G.: The global atmospheric electrical circuit and climate, Surv Geophys, 25, 441–484, 2004.

Harrison, R. G.: The carnegie curve, Surv Geophys, 34, 209–232, 2013.

Harrison, R. G.: Behind the curve: a comparison of historical sources for the Carnegie curve of the global atmospheric electric circuit, Hist Geo- Space Sci, 11, 207–213, https://doi.org/10.5194/hgss-11-207-2020, 2020.

Harrison, R. G. and Carslaw, K. S.: Ion-aerosol-cloud processes in the lower atmosphere, Rev Geophys, 41, https://doi.org/10.1029/2002RG000114, 2003.

Harrison, R. G. and Tammet, H.: Ions in the Terrestrial Atmosphere and Other Solar System Atmospheres, Space Sci Rev, 137, 107–118, https://doi.org/10.1007/s11214-008-9356-x, 2008.

Markson, R.: The global circuit intensity: Its measurement and variation over the last 50 years, B A Meteorol Soc, 88, 223–242, 2007.

Parkinson, W.: The diurnal variation of the electric potential of the atmosphere over the oceans, UGGI (Sect. Terr. Magn. Elec.), p. 340–341, 1931.

Price, C.: Global surface temperatures and the atmospheric electrical circuit, Geophys Res Lett, 20, 1363–1366, 1993.

Rycroft, M., Israelsson, S., and Price, C.: The global atmospheric electric circuit, solar activity and climate change, J Atmos Solar-Terr Phy, 62, 1563–1576, https://doi.org/10.1016/S1364-6826(00)00112-7, 2000.

Rycroft, M. J., Harrison, R. G., Nicoll, K. A., and Mareev, E. A.: An overview of earth's global electric circuit and atmospheric conductivity, Space Sci Rev, 137, 83–105, https://doi.org/10.1007/s11214-008-9368-6, 2008.

Torreson, O. W.: Ocean atmospheric-electric results, Oceanography III: Scientific results of Cruise VII during 1928-1929 under Command of Captain JP Ault, 1946.

Williams, E. R.: The global electrical circuit: A review , Atmos Res, 91, 140–152, https://doi.org/10.1016/j.atmosres.2008.05.018, 13th International Conference on Atmospheric ElectricityICAE 2007, 2009.

Wilson, C. T. R.: Investigations on lighting discharges and on the electric field of thunderstorms, Philosophical Transactions of the Royal Society of London. Series A, Containing Papers of a Mathematical or Physical Character, 221, 73–115, 1921.

WMO: Guide to Marine Meteorological Services (Appendix 2), Tech. rep., 2018.

Zafrir, H., Haquin, G., Malik, U., Barbosa, S., Piatibratova, O., and Steinitz, G.: Gamma versus alpha sensors for Rn-222 long-term monitoring in geological environments, Radiat Meas, 46, 611–620, https://doi.org/10.1016/j.radmeas.2011.04.027, 2011.